N-WASP is required for membrane wrapping and myelination by Schwann cells

Nurit Novak,[1] Vered Bar,[1] Helena Sabanay,[1] Shahar Frechter,[1] Martine Jaegle,[3] Scott B. Snapper,[2] Dies Meijer,[3] and Elior Peles[1]

[1]Department of Molecular Cell Biology, Weizmann Institute of Science, Rehovot 76100, Israel
[2]Gastrointestinal Unit, Massachusetts General Hospital, Boston, MA 02114
[3]Department of Cell Biology and Genetics, Erasmus University Medical Center, 3000 CA Rotterdam, Netherlands

During peripheral nerve myelination, Schwann cells sort larger axons, ensheath them, and eventually wrap their membrane to form the myelin sheath. These processes involve extensive changes in cell shape, but the exact mechanisms involved are still unknown. Neural Wiskott–Aldrich syndrome protein (N-WASP) integrates various extracellular signals to control actin dynamics and cytoskeletal reorganization through activation of the Arp2/3 complex. By generating mice lacking N-WASP in myelinating Schwann cells, we show that N-WASP is crucial for myelination. In N-WASP–deficient nerves, Schwann cells sort and ensheath axons, but most of them fail to myelinate and arrest at the promyelinating stage. Yet, a limited number of Schwann cells form unusually short internodes, containing thin myelin sheaths, with the occasional appearance of myelin misfoldings. These data suggest that regulation of actin filament nucleation in Schwann cells by N-WASP is crucial for membrane wrapping, longitudinal extension, and myelination.

Introduction

Myelination by Schwann cells in the peripheral nervous system (PNS) is essential for efficient saltatory conduction of action potentials. During myelination, Schwann cells undergo extensive morphological changes: cellular process extension and retraction, ensheathment, membrane wrapping, and compaction (Jessen and Mirsky, 2005). Schwann cells first extend cellular protrusions that sort larger axons designated to be myelinated (i.e., radial axonal sorting) and establish a 1:1 relationship with individual axons (Sherman and Brophy, 2005). Myelination then commences by wrapping the inner membrane of the Schwann cell around the axon (Bunge et al., 1989).

The dramatic changes in cell shape occurring during myelination likely depend on constant rearrangement of the actin cytoskeleton. It was demonstrated that ensheathment and myelination by Schwann cells in vitro are impaired by the actin polymerization inhibitor cytochalasin D (Fernandez-Valle et al., 1997). Similarly, Schwann cells associated with axons but failed to ensheath them in co-culture after blocking myosin II activity (Wang et al., 2008). Several studies have also indicated a role for members of the small Rho-GTPase family, Rac1, Cdc42, and RhoA, in PNS myelination (Feltri et al., 2008; Krause et al., 2008; Bauer et al., 2009). These GTPases regulate the assembly of filamentous actin in response to extracellular signaling (Hall, 1998; Etienne-Manneville and Hall, 2002). In the PNS, Rho/Rho kinase signaling regulates radial sorting (Pereira et al., 2009), suppresses branching, and controls internodal length by promoting the coordinated movement of the myelin sheath around the axon (Melendez-Vasquez et al., 2004). Rac1 and Cdc42 are required for radial axonal sorting; however, they operate by distinct mechanisms (Feltri et al., 2008; Krause et al., 2008). Rac1 is an effector of β1-integrins and is required for Schwann cell process extension (Benninger et al., 2007; Nodari et al., 2007). In contrast, Cdc42 does not affect process extension, and its deletion results in a sorting defect likely caused by the strong reduction in the number of

Correspondence to Elior Peles: peles@weizmann.ac.il

Abbreviations used in this paper: CAP, compound action potential; DHH, Desert Hedgehog; MBP, myelin basic protein; N-WASP, neural WASP; PNS, peripheral nervous system; WASP, Wiskott–Aldrich syndrome protein; WAVE, WASP family verprolin homologous.

The Rockefeller University Press $30.00
J. Cell Biol. Vol. 192 No. 2 243–250
www.jcb.org/cgi/doi/10.1083/jcb.201010013

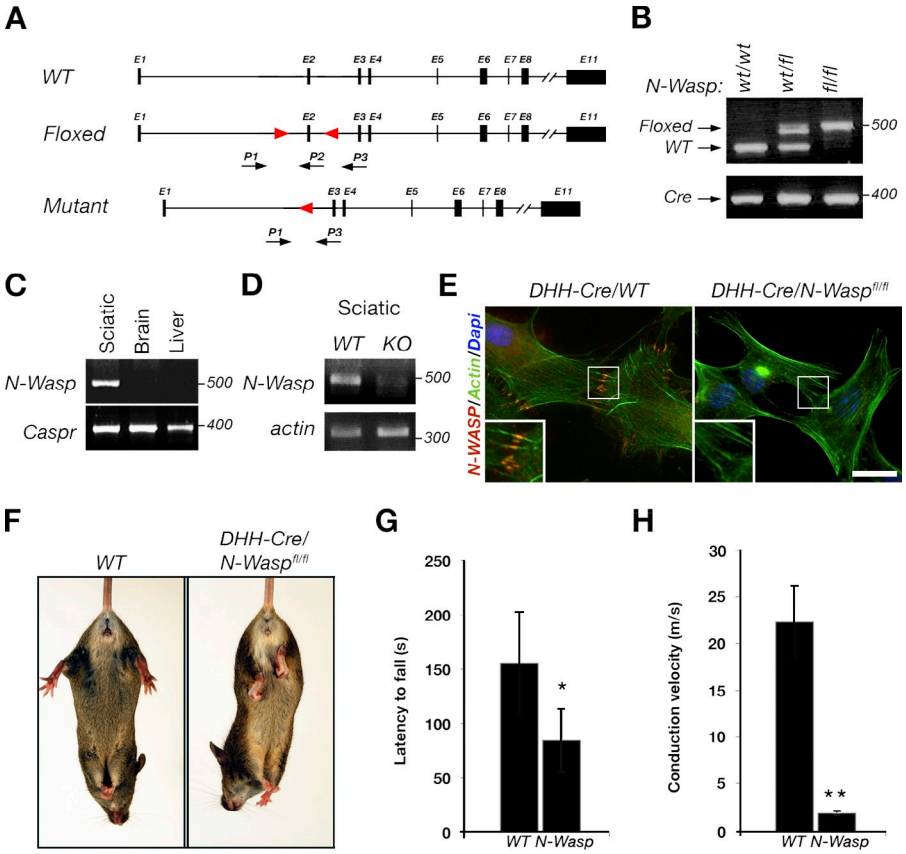

Figure 1. **Schwann cell–specific ablation of N-WASP results in motor abnormalities.** (A) Schematic representation of the genomic *N-Wasp* (*WT, wild type*), floxed, and mutant loci. The location of the exons (E1–E11), loxP sites (red triangles), and primers used for genotyping (P1–P3) are indicated. (B) PCR analysis of genomic tail DNA of wild type (*wt/wt*), heterozygous (*wt/fl*), or mutant (*fl/fl*) mice using primer sets that detect the wild-type and floxed *N-Wasp* alleles as well as the Cre gene. (C) Specific deletion of *N-Wasp* in Schwann cells. PCR analysis of genomic DNA from the indicated tissues of mutant mice using primers P1–P3 to N-WASP or Caspr as a control. (D) RT-PCR analysis of *N-Wasp* and *actin* using mRNA isolated from sciatic nerves of control (wild type) and mutant mice (KO, knockout). (B–D) Size markers are given in base pairs. (E) Labeling of wild-type and mutant Schwann cells using an antibody to N-WASP. Actin and nuclei were colabeled with phalloidin and DAPI, respectively. High magnification of the framed areas is shown in the insets. Bar, 50 µm. (F) *N-Wasp* mutant mice exhibit abnormal clasping of their hind limbs when lifted by their tails. (G) The rotarod test was performed with adult mice. Mutant mice (*N-Wasp*) had a shorter latency to fall compared with their littermate controls. Error bars represent the SD of $n = 4–6$ mice for each genotype (*, $P < 0.05$). (H) CAPs recorded from adult mice show a strong reduction in nerve conduction velocity in the mutant. Error bars represent the SD of $n = 5–8$ mice for each genotype (**, $P < 0.0005$).

Schwann cells (Benninger et al., 2007). In addition, Cdc42 may be required for membrane wrapping and transition from promyelinating to myelinating Schwann cells (Krause et al., 2008). In support of this idea, disruption of frabin/FGD4, a GTPase exchange factor that regulates Cdc42 activity (Umikawa et al., 1999), causes demyelinating Charcot–Marie–Tooth (CMT4H) neuropathy (Delague et al., 2007; Stendel et al., 2007).

Rac1 and Cdc42 GTPases catalyze actin polymerization by activating the Arp2/3 complex through downstream effectors belonging to the Wiskott–Aldrich syndrome protein (WASP) and WASP family verprolin homologous (WAVE) family of proteins (Stradal and Scita, 2006; Chhabra and Higgs, 2007; Takenawa and Suetsugu, 2007). WASP and WAVE proteins interact with the Arp2/3 complex and G-actin to promote actin filament nucleation and branching (Goley and Welch, 2006). Neural WASP (N-WASP) regulates filopodia formation and membrane invagination, whereas WAVE proteins serve as Rac1 effectors in the formation of lamellipodia (Takenawa and Suetsugu, 2007). WASP and WAVE proteins are expressed by Schwann cells, and inhibition of N-WASP in vitro blocked process extension by Schwann cells, suggesting that it may play a role in myelination (Bacon et al., 2007). Given that actin nucleation is a major driving force in membrane movement, we set to examine the role of N-WASP in myelination in vivo by generating mice specifically lacking this protein in Schwann cells. Our results suggest that N-WASP is essential for membrane wrapping and longitudinal extension of myelinating Schwann cells.

Results and discussion

Conditional ablation of N-WASP in Schwann cells

To study the role of N-WASP in PNS myelination, we generated mice lacking N-WASP in Schwann cells by using a conditional floxed allele of *N-Wasp*, in which the second coding exon was flanked by loxP sites (*N-Wasp*$^{fl/fl}$; Cotta-de-Almeida et al., 2007). Schwann cell–specific deletion of N-WASP was obtained by crossing *N-Wasp*$^{fl/fl}$ mice with Desert Hedgehog (DHH)–Cre transgenic mice (*DHH-Cre*), in which Cre is active in Schwann cell precursors from embryonic day 12.5 (E12.5; Jaegle et al., 2003). Genotyping of *DHH-Cre/N-Wasp*$^{fl/fl}$ (referred to herein as mutant mice) was determined by PCR analysis of tail DNA (Fig. 1, A and B). By performing PCR analysis of genomic DNA from different tissues, we show that N-WASP was specifically inactivated in the sciatic nerve but not in the brain or liver (Fig. 1 C). RT-PCR analysis performed on mRNA from sciatic nerves of control and mutant mice revealed a significant decrease of the N-WASP transcript in the mutant (Fig. 1 D). Residual levels of N-WASP mRNA still detected in mutant nerves are likely caused by its expression in perineurial fibroblasts. The absence of N-WASP in Schwann cells was evident by labeling of cells isolated from control and mutant mice (Fig. 1 E).

Impaired motor activity in mutant mice lacking N-WASP in myelinating glia

Homozygous mutant mice were viable but exhibited hypomotility, tremor, and progressive hind-limb paralysis. They displayed

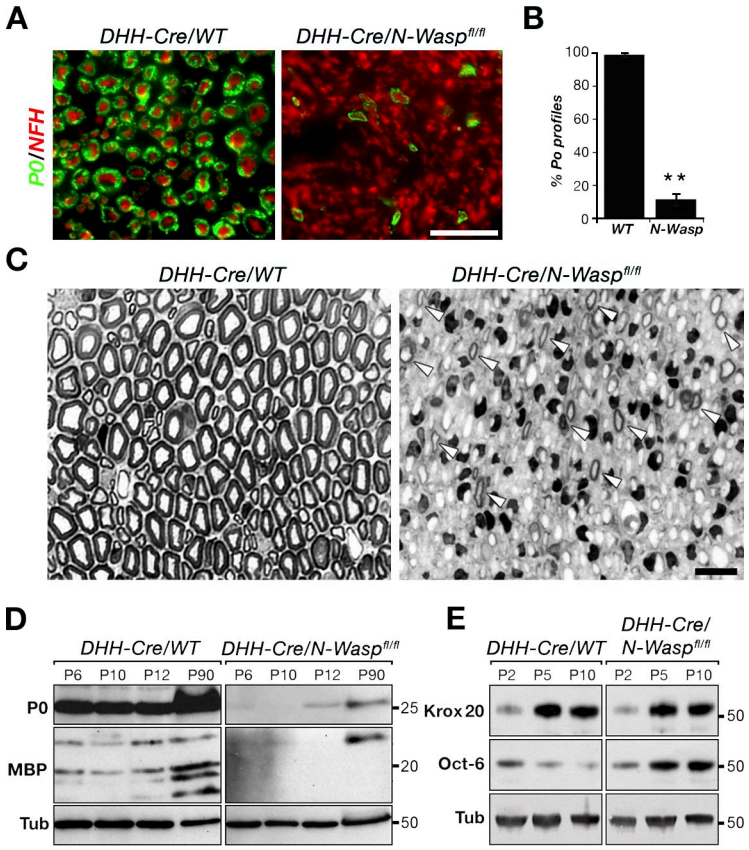

Figure 2. ***DHH-Cre/N-Wasp*$^{fl/fl}$ mice exhibit a severe PNS myelination defect.** (A) Transverse sections of P60 sciatic nerves from control and mutant mice immunolabeled with antibodies to P0 and neurofilament (NFH). Bar, 50 µm. (B) There was a strong reduction in the number of axons encircled by a P0-positive myelin sheath in the mutant. Error bars represent the SD of $n = 3$ mice for each genotype (**, $P < 0.0001$). (C) Transverse semithin sections of sciatic nerves isolated from control and mutant mice at P30 stained with toluidine blue. Although in the control nerve most axons were enveloped by a mature myelin sheath, only a few thin myelin profiles were detected in the mutant (arrowheads). Bar, 20 µm. (D and E) Western blot analysis of sciatic nerves from control and mutant mice at different ages using the indicated antibodies. Tubulin (Tub) served as a loading control. Molecular masses are given in kilodaltons. WT, wild type.

enhanced limb-clasping reflexes when suspended by the tail, whereas control mice extended their limbs (Fig. 1 F). These mutants had a shorter latency to fall from a rotarod, further indicating that the deletion of N-WASP in myelinating Schwann cells resulted in a severe motor coordination and balance defect (Fig. 1 G). The motor impairments correlated with a striking reduction in nerve conduction velocity in the mutant (Fig. 1 H) to the level of unmyelinated C fibers (Douglas and Ritchie, 1962).

DHH-Cre/N-Wasp$^{fl/fl}$ mice exhibit a severe PNS myelination defect

Immunofluorescence labeling of the sciatic nerve cross sections showed a large reduction in PO protein immunoreactivity compared with control nerves (Fig. 2, A and B). Toluidine blue–stained transverse semithin sections of P30 sciatic nerves revealed that the mutant nerves were severely hypomyelinated (Fig. 2 C). Although at this age control nerves were filled with myelinated axons, only a few thin myelin profiles were detected in the mutant. In addition, compared with control nerves, P30 mutant nerves had a higher density of Schwann cell nuclei. An increase in the number of Schwann cells was observed in several hypomyelinated mutants and is considered to be secondary to the defect in myelination (Koszowski et al., 1998; Court et al., 2004; Nodari et al., 2007). This conclusion was further supported by observations in mixed dorsal root ganglion cultures, in which there was no significant difference in the number of control and N-WASP–deficient Schwann cells (unpublished data). Consistent with the observed myelination impairment, the levels of two major myelin components in the PNS, P0 and myelin basic protein (MBP), were reduced in the mutant sciatic nerves (Fig. 2 D). The expression of Krox-20 was comparable between the mutant and control nerves, whereas the expression of Oct-6 was elevated in the mutant (Fig. 2 E). These results indicate that Schwann cells initiate the transcriptional program of myelination, but the vast majority fails to elaborate proper myelin.

By immunofluorescence labeling of teased sciatic nerves, we observed that myelin internodes formed only irregularly in the mutant compared with control mice (Fig. 3, A–D). To evaluate the extent of axonal coverage by myelin, we calculated the ratio between MBP-labeled internodes and axonal length. Although in control animals this ratio was 0.99 ± 0.01 as expected, in mutants it was reduced to 0.34 ± 0.32 (the high deviation from the mean reflects the variability of axon coverage by myelin), indicating a severe dysmyelination phenotype. In the absence of N-WASP, myelin internodes were occasionally found distant from each other on the same axon and were separated by several nonmyelinating Schwann cells (Fig. 3, B and C). MBP- or P0-labeled segments resembled the immature ("canoe" shape) morphology often seen in young myelinating co-cultures (Fig. 3 C). We also detected the presence of split internodes, in which the MBP immunoreactivity of a single internode appeared as two distinct segments with different intensities (Fig. 3 D). The border between two such segments was often accompanied by the accumulation of Caspr, an axonal paranodal junction component, in the underlying axon (Fig. 3 D), further indicating an abnormal process of myelination. Labeling of mutant nerves for P0 revealed that, in some internodes, the myelin sheath did not completely enwrap the axon (Fig. 3, E and F).

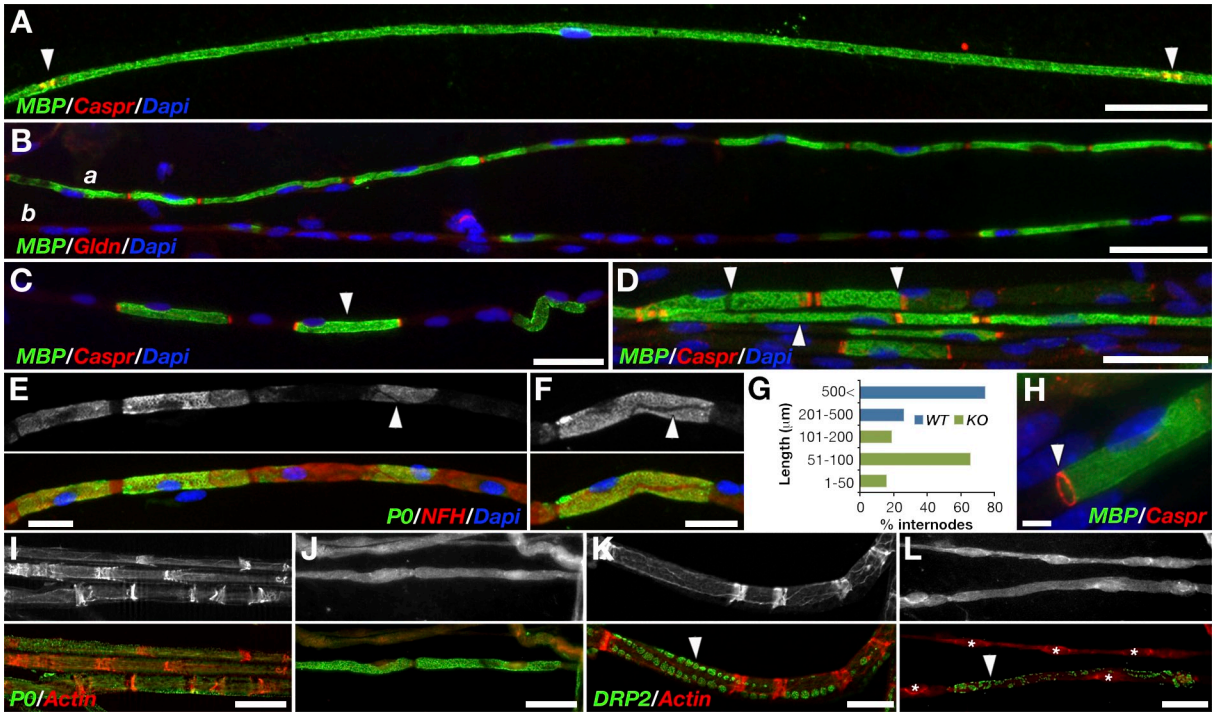

Figure 3. **N-WASP is required for membrane wrapping and longitudinal extension of the myelin unit.** (A) Fluorescence immunostaining of P30 teased sciatic nerve fibers of control mice using antibodies to MBP and Caspr (to label the paranodal junction; arrowheads). The internodal length is 563 µm. (B) Immunolabeling of teased sciatic nerve fibers of mutant mice using antibodies to MBP and gliomedin (Gldn). Axon a is almost completely (92%; 516–560 µm) covered by nine internodes with a mean length of 57.3 µm each (ranging from 33 to 74 µm), whereas only two internodes are present in axon b. The unmyelinated regions along the axon are associated with multiple Schwann cell nuclei (DAPI). (A and B) Bars, 50 µm. (C and D) Labeling of mutant sciatic nerves using antibodies to MBP and Caspr. The arrowhead in C marks the presence of an immature short (29 µm) internode. Three segments containing split MBP staining are marked with arrowheads in D. Internodal axonal Caspr staining is detected in the middle of the top right and bottom internodes. (E and F) Labeling of teased sciatic nerve fibers of mutant mice using antibodies to P0 and neurofilament (NFH). Note the presence of myelin sheaths that did not entirely enclose the axon (arrowheads). (G) Quantitation of the divergence of internodal length in wild-type (WT) and mutant mice, which is presented as a percentage of the total number of segments measured for each genotype. n = 100 and 17 segments for mutant and wild-type nerves, respectively. KO, knockout. (H) Caspr immunoreactivity (arrowhead) reflects the formation of a thin myelin sheath in the mutant. Bar, 5 µm. (I–L) Phalloidin labeling (actin) of control (I and K) and mutant sciatic nerves (J and L) together with antibodies to P0 (I and J) or DRP2 (K and L). Arrowheads mark the membrane appositions labeled by DRP2. The asterisks mark areas of Schwann cell nuclei. (C–F and I–L) Bars, 20 µm.

Mutant internodes were much shorter than controls and varied in length from 22 to 160 µm (mean, 76.8 ± 28.3 µm) compared with an internodal length of 362–840 µm (mean, 581.1 ± 105.5 µm) in the control (Fig. 3 G). Caspr, whose concentration at the axolemma reflects the turning of the myelin sheath during wrapping (Eisenbach et al., 2009; Pedraza et al., 2009), often appeared as a thin collar at the edge of the MBP-positive segment, further indicating that these short internodes have fewer layers of myelin (Fig. 3 H). Staining with phalloidin revealed a clear difference in filamentous actin between wild-type and mutant sciatic nerves (Fig. 3, I–L). Although in wild-type nerves it was enriched in Schmidt–Lanterman incisures, periaxonal membrane, outer and inner mesaxon, and paranodal loops as previously reported (Trapp et al., 1989), in mutant nerves it was weakly detected over the entire myelinating segments (Fig. 3 J). In Schwann cells that were associated with axons but failed to myelinate, filamentous actin was occasionally detected around the nucleus (Fig. 3, J and L). The absence of N-WASP resulted in a severe disorganization of DRP2-labeled abaxonal membrane appositions (Fig. 3, K and L), further indicating an impaired formation of the actin cytoskeleton (Court et al., 2009). These results suggest that N-WASP drives PNS myelination by controlling actin polymerization.

N-WASP is required for Schwann cell membrane wrapping and myelination

In preparation for myelination in the PNS, immature Schwann cells first sort larger caliber axons designated to be myelinated. As revealed by low magnification electron microscopy of sciatic nerves at different postnatal days (Fig. 4), radial axonal sorting has almost been completed by P5 in both mutant and control nerves (Fig. 4, A and E). However, whereas at this age the majority of Schwann cells that have ensheathed axons in control nerves proceeded with myelination (Fig. 4 A), in mutant nerves they rarely myelinated axons and were arrested at the promyelinating stage (Fig. 4 E). Myelin profiles around axons in the mutant nerves were hardly detected at P5 (1.9 ± 1.1%; Fig. 4, E and I) and P10 (0.9 ± 0.1%; Fig. 4, F and J) and noticed in 6.7 ± 2.7% of axons at P30 and in 16.1 ± 9.4% of the axons at P60 (Fig. 4, G, H, K, and L).

Ultrastructural electron microscopy analysis of *DHH-Cre/N-Wasp*$^{fl/fl}$ sciatic nerves at P2 revealed the presence of Schwann cells that were engaged with groups of axons and sent long processes that enveloped the bundle and sorted out larger axons (Fig. 5 A), indicating that N-WASP in Schwann cells is not required for radial axonal sorting. At this age, there were numerous Schwann cells that had already ensheathed axons

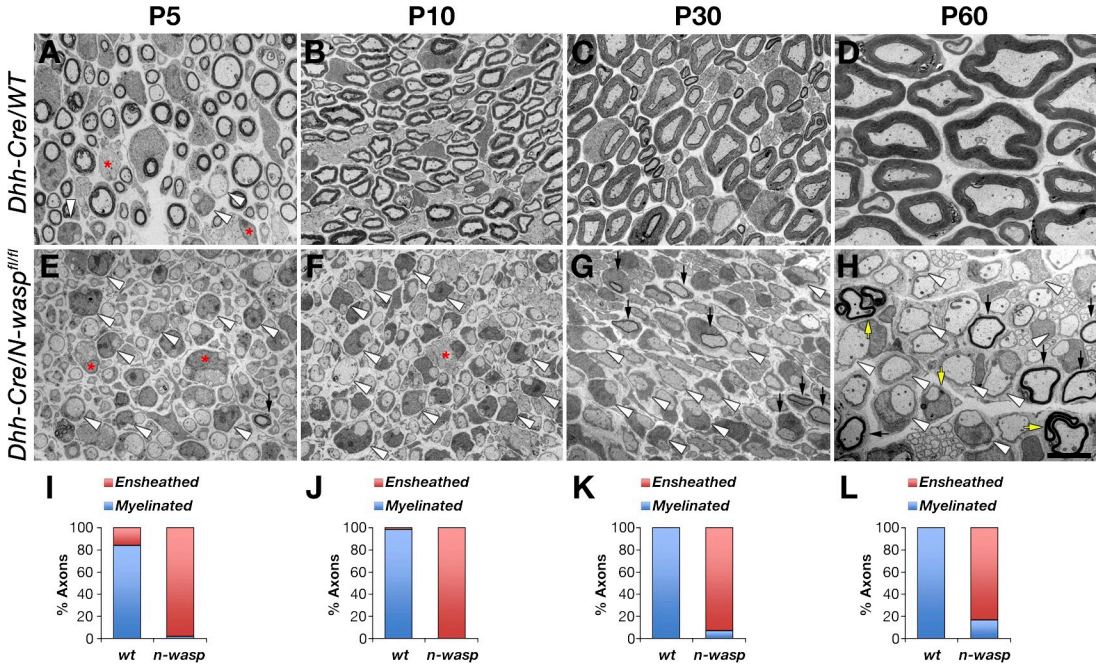

Figure 4. **Developmental analysis of peripheral nerves lacking N-WASP.** (A–H) Low magnification electron microscopy images of sciatic nerve cross sections from control (A–D) and mutant mice (E–H) at different postnatal days. (A) In control nerves at P5, most of the axons were already myelinated to some extent, and only a few bundles of unsorted axons (asterisks) or promyelinating Schwann cells (arrowheads) were detected. (E) In mutant nerves of the same age, radial sorting was almost complete as in control nerves, and only a few unsorted bundles (asterisks) were detected. Most of the Schwann cells established a 1:1 relationship with axons but failed to myelinate (arrowheads). (F–H) Analysis of the mutant nerves at P10 (F), P30 (G), and P60 (H) showed that most Schwann cells were arrested in the promyelinating stage throughout development (arrowheads). Myelin profiles around axons in the mutant nerves were rarely detected at P5 (E, black arrow) and were increasingly noticed as development progressed (G and H, black arrows). (H) Yellow arrows mark Schwann cells containing misfolded myelin in P60 nerves. (I–L) Percentage of ensheathed or myelinated axons in wild-type (wt) and mutant mice; $n = 3$ mice for each genotype at different ages ($P < 0.001$). Bars: (A–C and E–G) 7 µm; (D and H) 5 µm.

(Fig. 4, B and C). At P5, most of the mutant Schwann cells already established a 1:1 relationship with large axons but did not spiral their membrane around them to form myelin (Fig. 4, E and I; and Fig. 5 D). We also detected Schwann cells that produced conspicuous myelin lamellae that did not surround the axon (Fig. 5 D). The presence of such cells in the mutant may indicate that myelin membrane production and wrapping are interrelated, yet distinct, processes. In adult nerves, most of the Schwann cells were still arrested at the promyelinating stage, and only a fraction proceeded with myelination, usually producing thinner and abnormal myelin with apparent normal periodicity (Fig. 5, E and G; see also Fig. 4, D and H for a comparison of myelin thickness between mutant and control nerves). A prominent feature seen in adult mutant nerves was the presence of a redundant basal lamina around promyelinated (Fig. 5, F and H) as well as myelinated (Fig. 5 G) profiles, which reflects the repeating extension and retraction of Schwann cell processes. Finally, out of the Schwann cells that did myelinate axons in P30 and P60 mutant nerves, 48.0 ± 10.3 and 26.4 ± 7.3% (>600 axons per genotype; $n = 3$; $P < 0.005$) exhibited misfolding of the myelin sheath (Fig. 5, H–K). Such an aberrant myelin formation was not detected in age-matched wild-type control nerves. Examination of longitudinal sections of adult mutant sciatic nerves showed the presence of myelin outfoldings along internodes and at the nodes of Ranvier (Fig. 5, J and K).

Our data show that N-WASP is required for the generation of myelinated nerves in the PNS. Schwann cell–specific deletion of N-WASP causes severe dysmyelinating neuropathy characterized by motor deficiency and reduced nerve conduction velocity. We show that N-WASP is not required for axonal sorting but is essential for spiral wrapping of the membrane sheath by Schwann cells that have established a 1:1 relation with the axon. In adult mice lacking N-WASP, larger caliber axons were invariably ensheathed by single Schwann cells, but most of them did not myelinate and were arrested at this promyelinating stage. The role of N-WASP in membrane wrapping was further supported by the presence of myelin sheaths that only partially surrounded axons (Fig. 3, E and F; and Fig. 5 I), the split internodal appearance of MBP in the mutant (Fig. 3, D and E), and the abnormal localization of Caspr in myelinated axons in the adult animals (Fig. 3 D). Interestingly, inducible deletion of Cdc42 in Schwann cells (Krause et al., 2008) indicated that it is important for the transition from the promyelinating to the myelinating stage during remyelination, making it likely to regulate this process through N-WASP. Given that Cdc42 is activated by neuregulin (Benninger et al., 2007), N-WASP could provide a direct imperative link between ErbB2/3 receptor signaling and actin rearrangement during myelination.

In addition to its role in membrane wrapping, we found that N-WASP is also required for the longitudinal extension of the forming myelin internode. Thus, it appears that N-WASP fulfills several distinct functions in myelinating Schwann cells by promoting both spiral membrane wrapping and longitudinal growth of the myelin unit. Given its actin modulatory function

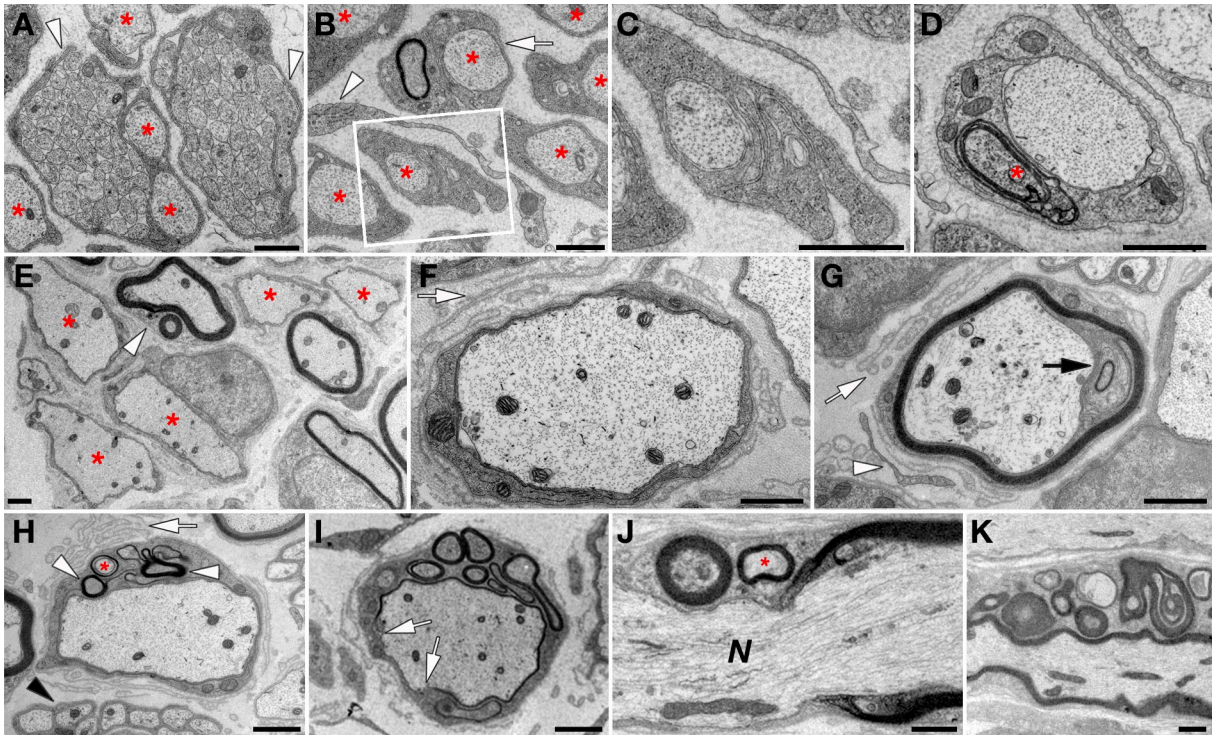

Figure 5. **Abnormalities detected in the PNS of N-WASP–deficient mice.** (A–K) Electron microscopy images showing sciatic nerve cross sections of *N-Wasp* mutants at P2 (A–C), P5 (D), and P60 (E–K). (A) Radial sorting is not impaired in the absence of N-WASP. Immature Schwann cells extend long processes (arrowheads) that envelop axon bundles and sort out large axons (asterisks). (B and C) At P2, many axons are sorted and ensheathed by Schwann cells (asterisks). An abnormal configuration of a single Schwann cell that surrounds a pair of axons, but only myelinates one of them (arrow), is shown in B. Higher magnification of the framed area is shown in C. A white arrowhead marks the presence of a perineurial fibroblast process. (D) A Schwann cell in a 1:1 relationship with an axon produces an abnormal myelin sheath not encircling the axon (asterisk). (E–I) Cross sections of mutant nerves at P60. (E) In the adult nerve, only a few Schwann cells myelinate, usually forming thinner myelin and occasionally containing outfolds (arrowhead), whereas many remain arrested at the promyelinating stage (asterisks). (F) Schwann cell that fails to myelinate its associated axon surrounded by empty, onion bulb–like basal lamina (arrow). (G) Aberrant loose myelin misfolding (black arrow) located between the axon and a thin (five layers) compact myelin sheath. Redundant basal lamina and a retracted cytoplasmic Schwann cell extension are labeled by a white arrow and arrowhead, respectively. (H) A large caliber axon ensheathed by a Schwann cell, which produces myelin profiles that are covered by its plasma membrane (white arrowheads). It also appears to form myelin around a thin axonal process (asterisk). Redundant basal lamina and Remak bundles are marked by an arrow and a black arrowhead, respectively. (I) A myelin sheath is not detected around the entire perimeter of a large caliber axon (arrows), which is reminiscent of the gap-containing myelin sheath seen in Fig. 3 F. The related Schwann cell produces numerous abnormal myelin misfoldings. (J and K) Longitudinal sections of mutant nerves at P60. Myelin outfolding and myelinated axonal process (asterisk) detected at the nodes (J) and the internodes (K). N, nodes of Ranvier. Bars, 1 µm.

as well as its ability to interact with membrane curvature–inducing proteins (Takenawa and Suetsugu, 2007), it is possible that, in addition to regulating Schwann cell membrane movement, N-WASP also affects myelination by regulating endocytic vesicle trafficking (Kaksonen et al., 2006). Endocytic recycling of myelin proteins has been implicated in central nervous system myelination (Trajkovic et al., 2006; Winterstein et al., 2008), and its importance in PNS myelination is supported by the identification of several Charcot–Marie–Tooth neuropathy genes, which encode for proteins involved in endocytosis and trafficking of membrane components (Niemann et al., 2006; Scherer and Wrabetz, 2008). The finding that N-WASP is required for membrane wrapping and Schwann cell extension provides a step further in our understanding of how actin-dependent cytoskeletal organization is regulated during PNS myelination.

Materials and methods

Generation of N-WASP conditional knockout mice

Generation of *DHH-Cre/N-Wasp*$^{fl/fl}$ (Cotta-de-Almeida et al., 2007) and *DHH-Cre* (Jaegle et al., 2003) mice was previously described. Homozygous *DHH-Cre/N-Wasp*$^{fl/fl}$ mice were obtained by a conventional breeding scheme. Genotypes were determined by performing PCR on genomic DNA extracted from mice tails or sciatic nerves using previously described primers (Lyubimova et al., 2010).

RNA analysis

Total RNA was isolated from sciatic nerves using TRI Reagent (Sigma-Aldrich). Transcribed cDNA was obtained with SuperScript reverse transcription II (Invitrogen). PCR was performed using N-WASP (5′-AGGGTCACCAACGTGGGC-3′ and 5′-GGTGTGGGAGATGTTGTTG-3′)– or actin (5′-GAGCACCCTGTGCTGCTCACCGAGG-3′ and 5′-GTGGTGGTGAAGCTGTAGCCACGCT-3′)–specific primers.

Electrophysiology and motor function

Compound action potential (CAP) measurements were performed as previously described (Cai et al., 2005). Mice (6–8 wk of age; $n = 5$–8) were anesthetized by ketamine/xylazine (1:10). Body temperature was maintained by placing the mice on a warm pad (34–38°C; DC temperature controller; FHC, Inc.). Signals were amplified, digitized, recorded, and analyzed using the pClamp10 program (MDS Analytical Technologies). CAP studies were performed by placing the recording electrodes proximally at the base of the tail, stimulating ∼5 cm distally, and averaging from 20 stimulations. All recordings were made with supramaximal stimulation. The stimulus amplitude required to detect CAP from N-WASP mutants was ∼10 times higher than the wild-type threshold amplitude. Conduction velocities were calculated based on the latency of the onset of the CAP and the measured distance between the stimulation site and recording site. The rotarod

motor test was performed using an accelerating rotarod. Mice (4–8 mice per group at 6–8 wk of age) were trained on a rotating drum (3-cm diameter, accelerating from 0 to 40 rpm in 4 min) for a consecutive 4 d. A day later, the mean latency to fall of each mouse was measured in three subsequent trials.

Electron microscopy

Sciatic nerves were fixed and processed as previously described (Feinberg et al., 2010) and examined using a transmission electron microscope (CM-12; FEI) coupled with a camera (Eagle 2K×2K; FEI). Semithin sections were stained with toluidine blue for analysis under a light microscope (Axioskop 2; Carl Zeiss, Inc.).

Cell culture

Myelinating dorsal root ganglion cultures were obtained as previously described (Eshed et al., 2005). Mouse Schwann cell cultures were obtained from P0–P2 sciatic nerves. Nerves were digested in enzyme buffer containing 0.7 mg/ml collagenase type I in 0.25% trypsin (Invitrogen) as previously described (Benninger et al., 2007). After trituration, cells were grown on poly-D-lysine/laminin-coated dishes (Sigma-Aldrich) in DME/F12 medium (Invitrogen) containing 10% conditioned medium of CHO cells expressing neuregulin, 4 µM forskolin (Sigma-Aldrich), penicillin + streptomycin (Invitrogen), sodium pyruvate (Invitrogen), and 30% rat Schwann cell–conditioned medium.

Immunostaining, Western blotting, and antibodies

Teased sciatic nerves and frozen sections were prepared and labeled as previously described (Spiegel et al., 2007) and mounted in elvanol. Fluorescence images were obtained using a microscope (Axioskop 2) equipped with 10×/0.3 Ph1, 20×/0.5 NA, 40×/1.3 NA, and 63×/1.4 NA Plan Neofluar objectives. Images were acquired using a charge-coupled device camera (ORCA-ER; Hamamatsu) controlled by acquisition software (Axiovision 4.7; Carl Zeiss, Inc.). Processing of the images was performed using Photoshop software (CS3; Adobe). Quantification of the myelin segments was performed using image analysis software (Volocity 4.2.1; PerkinElmer). Primary antibodies used in this study were rat anti-MBP (Millipore), rat antineurofilament (Millipore), rabbit anti-Caspr (Peles et al., 1997), rabbit anti-P0 (Wong and Filbin, 1994), rabbit antigliomedin (Eshed et al., 2005), rabbit anti-DRP2 (Sherman et al., 2001), rabbit anti–Oct-6 (Jaegle et al., 2003), and rabbit anti–Krox-20 (Darbas et al., 2004). The N-WASP antibody (H-100; Santa Cruz Biotechnology, Inc.) we used recognizes amino acids 111–210 of N-WASP, which are located downstream of the deleted exon (amino acids 38–81). Phalloidin-568–, phalloidin-488–, and Alexa Fluor 488–coupled anti–rabbit were purchased from Invitrogen. Cy3-coupled anti–rabbit, Cy3-coupled anti–mouse, and Cy5-coupled anti–rat were obtained from Jackson ImmunoResearch Laboratories, Inc. For Western blot analysis, sciatic nerves were dissected, snap frozen in liquid nitrogen, and extracted in Laemmli sample buffer as previously described (Jaegle et al., 2003).

Quantitation and statistical analysis

The number of myelinating profiles shown in Fig. 2 B was calculated by counting >1,000 neurofilament-labeled axons from three different animals of each genotype. The ratio between MBP-labeled internodes and axonal length was calculated by dividing the total length of myelin internodes present on an axonal segment by its overall length (n = 100 for mutants and 17 for wild type). The number of ensheathing and myelinating Schwann cells at different ages (Fig. 4, I–L) was determined by counting at least 1,300 fibers from each genotype from three mice. In experiments in which multiple samples were compared, the statistical significance was determined using the two-tailed t test according to the Bonferroni correction.

We would like to thank Peter Brophy and Marie Filbin for antibodies and Eyal Schejter and Diane Sherman for their insightful suggestions.

This work was supported by grants from the National Institutes of Health (NS50220 to E. Peles and 5P01 HL59561 to S.B. Snapper), the Dr. Miriam and Sheldon G. Adelson Medical Research Foundation, the Israel Science Foundation, the Shapell Family Biomedical Research Foundation at the Weizmann Institute, the Moskowitz Center for Imaging, and the European Community's Seventh Framework Program (FP7/2007–2013; HEALTH-F2-2008-201535 to E. Peles and D. Meijer). E. Peles is the Incumbent of the Hanna Hertz Professorial Chair for Multiple Sclerosis and Neuroscience.

Submitted: 4 October 2010
Accepted: 21 December 2010

References

Bacon, C., V. Lakics, L. Machesky, and M. Rumsby. 2007. N-WASP regulates extension of filopodia and processes by oligodendrocyte progenitors, oligodendrocytes, and Schwann cells-implications for axon ensheathment at myelination. *Glia.* 55:844–858. doi:10.1002/glia.20505

Bauer, N.G., C. Richter-Landsberg, and C. Ffrench-Constant. 2009. Role of the oligodendroglial cytoskeleton in differentiation and myelination. *Glia.* 57:1691–1705. doi:10.1002/glia.20885

Benninger, Y., T. Thurnherr, J.A. Pereira, S. Krause, X. Wu, A. Chrostek-Grashoff, D. Herzog, K.A. Nave, R.J. Franklin, D. Meijer, et al. 2007. Essential and distinct roles for cdc42 and rac1 in the regulation of Schwann cell biology during peripheral nervous system development. *J. Cell Biol.* 177:1051–1061. doi:10.1083/jcb.200610108

Bunge, R.P., M.B. Bunge, and M. Bates. 1989. Movements of the Schwann cell nucleus implicate progression of the inner (axon-related) Schwann cell process during myelination. *J. Cell Biol.* 109:273–284. doi:10.1083/jcb.109.1.273

Cai, H., X. Lin, C. Xie, F.M. Laird, C. Lai, H. Wen, H.C. Chiang, H. Shim, M.H. Farah, A. Hoke, et al. 2005. Loss of ALS2 function is insufficient to trigger motor neuron degeneration in knock-out mice but predisposes neurons to oxidative stress. *J. Neurosci.* 25:7567–7574. doi:10.1523/JNEUROSCI.1645-05.2005

Chhabra, E.S., and H.N. Higgs. 2007. The many faces of actin: matching assembly factors with cellular structures. *Nat. Cell Biol.* 9:1110–1121. doi:10.1038/ncb1007-1110

Cotta-de-Almeida, V., L. Westerberg, M.H. Maillard, D. Onaldi, H. Wachtel, P. Meelu, U.I. Chung, R. Xavier, F.W. Alt, and S.B. Snapper. 2007. Wiskott Aldrich syndrome protein (WASP) and N-WASP are critical for T cell development. *Proc. Natl. Acad. Sci. USA.* 104:15424–15429. doi:10.1073/pnas.0706881104

Court, F.A., D.L. Sherman, T. Pratt, E.M. Garry, R.R. Ribchester, D.F. Cottrell, S.M. Fleetwood-Walker, and P.J. Brophy. 2004. Restricted growth of Schwann cells lacking Cajal bands slows conduction in myelinated nerves. *Nature.* 431:191–195. doi:10.1038/nature02841

Court, F.A., J.E. Hewitt, K. Davies, B.L. Patton, A. Uncini, L. Wrabetz, and M.L. Feltri. 2009. A laminin-2, dystroglycan, utrophin axis is required for compartmentalization and elongation of myelin segments. *J. Neurosci.* 29:3908–3919. doi:10.1523/JNEUROSCI.5672-08.2009

Darbas, A., M. Jaegle, E. Walbeehm, H. van den Burg, S. Driegen, L. Broos, M. Uyl, P. Visser, F. Grosveld, and D. Meijer. 2004. Cell autonomy of the mouse claw paw mutation. *Dev. Biol.* 272:470–482. doi:10.1016/j.ydbio.2004.05.017

Delague, V., A. Jacquier, T. Hamadouche, Y. Poitelon, C. Baudot, I. Boccaccio, E. Chouery, M. Chaouch, N. Kassouri, R. Jabbour, et al. 2007. Mutations in FGD4 encoding the Rho GDP/GTP exchange factor FRABIN cause autosomal recessive Charcot-Marie-Tooth type 4H. *Am. J. Hum. Genet.* 81:1–16. doi:10.1086/518428

Douglas, W.W., and J.M. Ritchie. 1962. Mammalian nonmyelinated nerve fibers. *Physiol. Rev.* 42:297–334.

Eisenbach, M., E. Kartvelishvily, Y. Eshed-Eisenbach, T. Watkins, A. Sorensen, C. Thomson, B. Ranscht, S.C. Barnett, P. Brophy, and E. Peles. 2009. Differential clustering of Caspr by oligodendrocytes and Schwann cells. *J. Neurosci. Res.* 87:3492–3501. doi:10.1002/jnr.22157

Eshed, Y., K. Feinberg, S. Poliak, H. Sabanay, O. Sarig-Nadir, I. Spiegel, J.R. Bermingham Jr., and E. Peles. 2005. Gliomedin mediates Schwann cell-axon interaction and the molecular assembly of the nodes of Ranvier. *Neuron.* 47:215–229. doi:10.1016/j.neuron.2005.06.026

Etienne-Manneville, S., and A. Hall. 2002. Rho GTPases in cell biology. *Nature.* 420:629–635. doi:10.1038/nature01148

Feinberg, K., Y. Eshed-Eisenbach, S. Frechter, V. Amor, D. Salomon, H. Sabanay, J.L. Dupree, M. Grumet, P.J. Brophy, P. Shrager, and E. Peles. 2010. A glial signal consisting of gliomedin and NrCAM clusters axonal Na^+ channels during the formation of nodes of Ranvier. *Neuron.* 65:490–502. doi:10.1016/j.neuron.2010.02.004

Feltri, M.L., U. Suter, and J.B. Relvas. 2008. The function of RhoGTPases in axon ensheathment and myelination. *Glia.* 56:1508–1517. doi:10.1002/glia.20752

Fernandez-Valle, C., D. Gorman, A.M. Gomez, and M.B. Bunge. 1997. Actin plays a role in both changes in cell shape and gene-expression associated with Schwann cell myelination. *J. Neurosci.* 17:241–250.

Goley, E.D., and M.D. Welch. 2006. The ARP2/3 complex: an actin nucleator comes of age. *Nat. Rev. Mol. Cell Biol.* 7:713–726. doi:10.1038/nrm2026

Hall, A. 1998. Rho GTPases and the actin cytoskeleton. *Science.* 279:509–514. doi:10.1126/science.279.5350.509

Jaegle, M., M. Ghazvini, W. Mandemakers, M. Piirsoo, S. Driegen, F. Levavasseur, S. Raghoenath, F. Grosveld, and D. Meijer. 2003. The POU

proteins Brn-2 and Oct-6 share important functions in Schwann cell development. *Genes Dev.* 17:1380–1391. doi:10.1101/gad.258203

Jessen, K.R., and R. Mirsky. 2005. The origin and development of glial cells in peripheral nerves. *Nat. Rev. Neurosci.* 6:671–682. doi:10.1038/nrn1746

Kaksonen, M., C.P. Toret, and D.G. Drubin. 2006. Harnessing actin dynamics for clathrin-mediated endocytosis. *Nat. Rev. Mol. Cell Biol.* 7:404–414. doi:10.1038/nrm1940

Koszowski, A.G., G.C. Owens, and S.R. Levinson. 1998. The effect of the mouse mutation claw paw on myelination and nodal frequency in sciatic nerves. *J. Neurosci.* 18:5859–5868.

Krause, S., C. Stendel, J. Senderek, J.B. Relvas, and U. Suter. 2008. Small Rho GTPases are key regulators of peripheral nerve biology in health and disease. *J. Peripher. Nerv. Syst.* 13:188–199. doi:10.1111/j.1529-8027.2008.00177.x

Lyubimova, A., J.J. Garber, G. Upadhyay, A. Sharov, F. Anastasoaie, V. Yajnik, G. Cotsarelis, G.P. Dotto, V. Botchkarev, and S.B. Snapper. 2010. Neural Wiskott-Aldrich syndrome protein modulates Wnt signaling and is required for hair follicle cycling in mice. *J. Clin. Invest.* 120:446–456. doi:10.1172/JCI36478

Melendez-Vasquez, C.V., S. Einheber, and J.L. Salzer. 2004. Rho kinase regulates schwann cell myelination and formation of associated axonal domains. *J. Neurosci.* 24:3953–3963. doi:10.1523/JNEUROSCI.4920-03.2004

Niemann, A., P. Berger, and U. Suter. 2006. Pathomechanisms of mutant proteins in Charcot-Marie-Tooth disease. *Neuromolecular Med.* 8:217–242. doi:10.1385/NMM:8:1:217

Nodari, A., D. Zambroni, A. Quattrini, F.A. Court, A. D'Urso, A. Recchia, V.L. Tybulewicz, L. Wrabetz, and M.L. Feltri. 2007. β1 integrin activates Rac1 in Schwann cells to generate radial lamellae during axonal sorting and myelination. *J. Cell Biol.* 177:1063–1075. doi:10.1083/jcb.200610014

Pedraza, L., J.K. Huang, and D. Colman. 2009. Disposition of axonal caspr with respect to glial cell membranes: implications for the process of myelination. *J. Neurosci. Res.* 87:3480–3491. doi:10.1002/jnr.22004

Peles, E., M. Nativ, M. Lustig, M. Grumet, J. Schilling, R. Martinez, G.D. Plowman, and J. Schlessinger. 1997. Identification of a novel contactin-associated transmembrane receptor with multiple domains implicated in protein-protein interactions. *EMBO J.* 16:978–988. doi:10.1093/emboj/16.5.978

Pereira, J.A., Y. Benninger, R. Baumann, A.F. Gonçalves, M. Ozçelik, T. Thurnherr, N. Tricaud, D. Meijer, R. Fässler, U. Suter, and J.B. Relvas. 2009. Integrin-linked kinase is required for radial sorting of axons and Schwann cell remyelination in the peripheral nervous system. *J. Cell Biol.* 185:147–161. doi:10.1083/jcb.200809008

Scherer, S.S., and L. Wrabetz. 2008. Molecular mechanisms of inherited demyelinating neuropathies. *Glia.* 56:1578–1589. doi:10.1002/glia.20751

Sherman, D.L., and P.J. Brophy. 2005. Mechanisms of axon ensheathment and myelin growth. *Nat. Rev. Neurosci.* 6:683–690. doi:10.1038/nrn1743

Sherman, D.L., C. Fabrizi, C.S. Gillespie, and P.J. Brophy. 2001. Specific disruption of a schwann cell dystrophin-related protein complex in a demyelinating neuropathy. *Neuron.* 30:677–687. doi:10.1016/S0896-6273(01)00327-0

Spiegel, I., K. Adamsky, Y. Eshed, R. Milo, H. Sabanay, O. Sarig-Nadir, I. Horresh, S.S. Scherer, M.N. Rasband, and E. Peles. 2007. A central role for Necl4 (SynCAM4) in Schwann cell-axon interaction and myelination. *Nat. Neurosci.* 10:861–869. doi:10.1038/nn1915

Stendel, C., A. Roos, T. Deconinck, J. Pereira, F. Castagner, A. Niemann, J. Kirschner, R. Korinthenberg, U.P. Ketelsen, E. Battaloglu, et al. 2007. Peripheral nerve demyelination caused by a mutant Rho GTPase guanine nucleotide exchange factor, frabin/FGD4. *Am. J. Hum. Genet.* 81:158–164. doi:10.1086/518770

Stradal, T.E., and G. Scita. 2006. Protein complexes regulating Arp2/3-mediated actin assembly. *Curr. Opin. Cell Biol.* 18:4–10. doi:10.1016/j.ceb.2005.12.003

Takenawa, T., and S. Suetsugu. 2007. The WASP-WAVE protein network: connecting the membrane to the cytoskeleton. *Nat. Rev. Mol. Cell Biol.* 8:37–48. doi:10.1038/nrm2069

Trajkovic, K., A.S. Dhaunchak, J.T. Goncalves, D. Wenzel, A. Schneider, G. Bunt, K.A. Nave, and M. Simons. 2006. Neuron to glia signaling triggers myelin membrane exocytosis from endosomal storage sites. *J. Cell Biol.* 172:937–948. doi:10.1083/jcb.200509022

Trapp, B.D., S.B. Andrews, A. Wong, M. O'Connell, and J.W. Griffin. 1989. Co-localization of the myelin-associated glycoprotein and the microfilament components, F-actin and spectrin, in Schwann cells of myelinated nerve fibres. *J. Neurocytol.* 18:47–60. doi:10.1007/BF01188423

Umikawa, M., H. Obaishi, H. Nakanishi, K. Satoh-Horikawa, K. Takahashi, I. Hotta, Y. Matsuura, and Y. Takai. 1999. Association of frabin with the actin cytoskeleton is essential for microspike formation through activation of Cdc42 small G protein. *J. Biol. Chem.* 274:25197–25200. doi:10.1074/jbc.274.36.25197

Wang, H., A. Tewari, S. Einheber, J.L. Salzer, and C.V. Melendez-Vasquez. 2008. Myosin II has distinct functions in PNS and CNS myelin sheath formation. *J. Cell Biol.* 182:1171–1184. doi:10.1083/jcb.200802091

Winterstein, C., J. Trotter, and E.M. Krämer-Albers. 2008. Distinct endocytic recycling of myelin proteins promotes oligodendroglial membrane remodeling. *J. Cell Sci.* 121:834–842. doi:10.1242/jcs.022731

Wong, M.H., and M.T. Filbin. 1994. The cytoplasmic domain of the myelin P0 protein influences the adhesive interactions of its extracellular domain. *J. Cell Biol.* 126:1089–1097. doi:10.1083/jcb.126.4.1089